On-chip Wireless Optical Channel Modeling for Massive Multi-core Computing Architectures

Mona Nafari, **Liang Feng** and **Josep Miquel Jornet**

Department of Electrical Engineering. University at Buffalo, The State University of New York
Buffalo, NY 14260, USA, E-mail: monanafa, fengl, jmjornet@buffalo.edu

***Abstract*—Wireless Networks on Chip (WNoC) consist of multiple independent cores interconnected by a smart combination of wired and wireless links. Wired interconnections have progressively moved from electrical tracks to nanophotonic waveguides in order to meet the demand for faster links. However, wireless links still largely rely on radio-frequency, millimeter-wave and, more recently, Terahertz-band communication, which offer a significantly lower bandwidth than their wired counterparts. To overcome this limitation, in light of the state of the art in optical nano-antennas, the use of wireless optical communication on-chip is proposed in this paper for the first time. Wireless optical links across cores can meet the demand for much higher data rates among cores, provide seamless wired and wireless transitions, and support multicast and broadcast transmissions among cores enabled by omnidirectional nano-antennas. To analyze the feasibility of this paradigm, in this paper, a multi-path channel model for on-chip light propagation is developed. More specifically, first, the channel frequency response in the case of line-of-sight propagation is obtained, by capturing the impact of spreading and absorption of light in silicon-based semiconductor materials. Then, the non-line-of-sight paths created by reflection at the material layer interfaces and diffraction at the core edges are modeled. Finally, a multi-path channel model is formulated, validated by means of electromagnetic simulations with COMSOL Multi-physics and utilized to analyze the main properties of on-chip wireless optical communication.**

***Index Terms*—Wireless Network on Chip; Wireless Optical Communications; Channel Modeling; Nanonetworks**

I. Introduction

Multicore architectures have become the dominant trend for both conventional and high-performance computing. These architectures consist of the interconnection of several independent processors or cores, including central processing units, graphic processing units and memory units. Control signaling and data sharing among cores requires reliable and energy efficient communication mechanisms among cores. As the number of cores within these processing systems increases, their communication needs rise dramatically and can become a major bottleneck for the overall system performance.

Similarly to the evolution of computer networks, shared bus architectures among cores have been progressively replaced by on-chip wires, switches and routers [1]. The resulting networks-on-chip or NoCs are designed by following similar principles and methods as those followed in traditional computer networks, but with different underlying communication technologies, networking architectures and system-wide objectives [2]. However, NoCs enabled by traditional electrical interconnects present fundamental limitations that point toward a reduced scalability beyond several tens of cores.

As a consequence of such limited scalability, considerable research efforts have been directed toward extending the original concept of NoC to other interconnect technologies. Diverse examples can be found in the literature, including the employment of vertical vias within stacked architectures [3], on-chip transmission lines for the transmission of modulated RF signals [4], or, more recently, nanophotonic interconnects enabling wired optical on-chip communication [5]. Indeed, optical on-chip communication has been proposed mainly due to its outstanding bandwidth and energy consumption capabilities with CMOS compatibility and reduced area footprint. However, the feasibility of an "all-wired" architecture decays quickly as the number of cores increases due to the challenges in creating point-to-point communication between elements or the limitations of wired architectures to support multi-cast and broadcast transmissions, among others.

To overcome such limitation, Wireless NoCs (WNoCs) with native broadcast and multicast capabilities thanks to integrated antennas have been proposed [6]. For the time being, different wireless communication technologies have been considered, including Impulse-Radio Ultra-Wide-Band (3.1-10.6 GHz) [7], Millimeter Waves (30-300 GHz) [8], and, more recently, Terahertz-band (0.1-10 THz) communication enabled by novel graphene plasmonic structures [9]. By increasing the communication frequency, the benefits are twofold. First, the higher the frequency, the smaller the footprint of the transceiver and antenna, and, thus, the easier the integration in the system. Second, the higher the frequency, the larger the available transmission bandwidth and, thus, the higher the achievable data rates. Motivated by these observations, and thinking of further miniaturizing existing integrated antennas and increasing the interconnect throughput, one question arises: could we create wireless optical links on-chip?

For many years, the challenges in fabricating precise structures smaller or at least comparable to the optical wavelengths limited the possibility of developing antennas "for light". However, within the last decade, the field of optical nano-antennas has experienced a major revolution [10]–[12]. Optical nano-antennas allow us to control the radiation of light in a similar fashion as traditional antennas for lower frequencies have done. Therefore, concepts such as wirelessly multicasting and broadcasting information at optical frequencies becomes

978-1-5090-4183-1/17/$31.00 ©2017 IEEE

a possibility. In addition, the available bandwidth at optical frequencies and the possibility to perform multiplexing ensure very high individual data-rates as well as aggregated network capacities. Moreover, compared to other high-throughput wireless technologies, such as graphene-enabled THz communication, the field of integrated photonics is much more mature. For example, micro and nano cavity lasers [13]–[15], detectors, power harvesting nano-devices [16, 17], nanosensors [18], and modulators [19] have been experimentally demonstrated. Ultimately, the use of "all optics" would allow us to seamlessly integrate optical wired and wireless links on chip.

Motivated by these results, we think of wireless optical communication as a new technology for WNoCs. Still, there are many research challenges to address, which range from the integration of nanophotonic sources, modulators, antennas and detectors on chip, to the development of practical communication and networking solutions for on-chip networks tailored to light communication. Among others, in order to analyze the feasibility of this approach, it is necessary to understand the propagation properties of on-chip wireless optical signals. Existing channel models cannot directly be utilized in this new paradigm. On the one hand, channel models for lower frequency bands such as [20, 21] do not capture the propagation phenomena affecting optical signals, including absorption, reflection and diffraction. Similarly, the existing channel models for free-space wireless optical systems do not capture the impact of material transitions in chip or diffraction at the core edges.

In this paper, we develop a multi-path channel model for on-chip light propagation. More specifically, first, we develop a mathematical framework to model the multi-path propagation of wireless optical signals on chip. On the one hand, the channel frequency response in the case of line-of-sight (LoS) propagation is obtained by analyzing the impact of spreading and absorption of light in silicon-based semiconductor materials. On the other hand, the non-line-of-sight (NLoS) paths created by reflection at the material layer interfaces and diffraction at the core edges are modeled. The developed analytical model is validated by means of frequency domain electromagnetic (EM) simulations with COMSOL Multi-physics [22]. The validated model is then utilized to analyze the main properties of on-chip wireless optical communication.

The remainder of this paper is organized as follows. In Sec. II, the multi-path channel model is analytically derived, by taking both into account LoS and NLoS propagation. The model is validated by means of simulations in Sec. III, and numerical results are provided to illustrate the behavior of the on-chip wireless optical channel. Finally, the paper is concluded in Sec. IV.

II. Multi-path Channel Model

To enable practical wireless optical communication in WNoCs, we need to understand and characterize the main phenomena affecting the propagation of such signals. In Fig. 1, we illustrate a side view of a silicon chip, with the standard layer thickness and material properties. In this section, we develop a multi-path channel model by taking into account both line-of-sight (Fig. 4(d)) and non-line-of-sight rays on-chip.

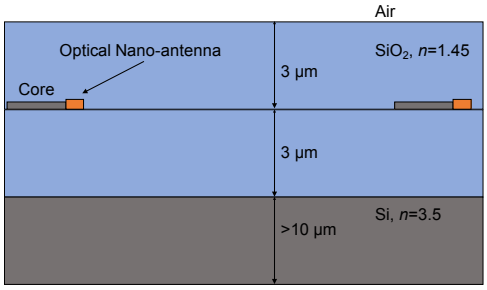

Fig. 1. Side view of the propagation medium, i.e., a standard CMOS chip.

A. Line-of-sight Propagation

The two main phenomena affecting the line of sight propagation of wireless optical signals are the spreading loss and the absorption loss. More specifically, the channel frequency response H_{LoS} is given by

$$H_{LoS}(f,d) = H_{spr}(f,d)H_{abs}(f,d), \tag{1}$$

where f refers to frequency, d stands for distance, and H_{spr} and H_{abs} are the spreading loss and the absorption loss, respectively.

1) Absorption in SiO_x: When EM radiation interacts with a semiconductor (SiO_x in our case), the optical properties of the material are revealed. The optical properties utilized to describe semiconductors are the absorption index, the refractive index and the band-gap. The absorption coefficient measures the distance photons travel within a material before being absorbed, and depends on the radiation frequency or, equivalently, the photon energy $E = hf$, where h is the Planck's constant. In our application scenario, the optical absorption coefficient K of SiO_x is given by [23, 24]:

$$K = \alpha_0 e^{\frac{(E-E_1)}{E_0}}, \tag{2}$$

where $\alpha_0 = 1.5 \cdot 10^6$ cm^{-1}, $E_1 = 2.2$ eV and E_0= 65meV. These have been determined from by a least-squares fit of (2) to the experimentally measured data in the absorption range of $K < 5 \cdot 10^3 cm^{-1}$ [23]. In Fig. 2, we illustrate the optical absorption coefficient K as a function of frequency. From the figure, it is clear that as the oxygen content increases, the band-gap increases and absorption decreases, such that for a given frequency, absorption coefficient of Si is higher than that of SiO_2. Finally, from the absorption coefficient, the absorption loss can be computed as:

$$H_{abs}(f,d) = \exp\left(-\frac{1}{2}K(f)\,d\right). \tag{3}$$

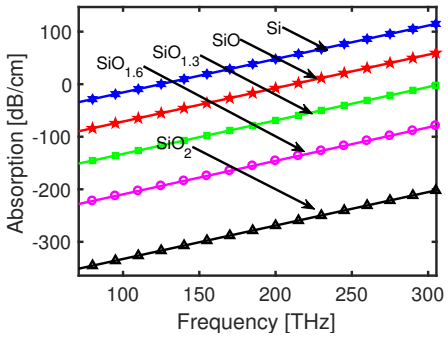

Fig. 2. Absorption coefficient K

2) Spreading: The spreading loss H_{spr} accounts for the attenuation due to the expansion of a wave as it propagates through the medium. Existing optical nano-antennas demonstrated to date resemble miniature dipole antennas and radiate almost isotropically [11, 25, 26]. Therefore, the assumption of spherical propagation, the spreading loss can be obtained as

$$H_{spr}(f,d) = \left(\frac{\frac{c}{n}}{\sqrt{4\pi} f d}\right) \exp\left(-j2\pi \frac{fd}{\frac{c}{n}}\right), \tag{4}$$

where c stands for the speed of light in vacuum, and n is the refractive index of the medium. The refractive index of SiO_x is given by [27]:

$$n = 0.9\sqrt{\frac{E_0.E_d}{E_0^2 - E^2}} + 1, \tag{5}$$

where E_d =17.15 eV is the dispersion energy and E_0 = 11.5 eV is the average excitation energy. The LOS rays are depicted in Fig. 4(a).

B. Non-line-of-sight Propagation

In addition to the LoS path, NLoS paths occur both due to the reflections at the interface between material layers as well as due to diffraction on the on-chip cores. We next formulate an analytical model for NLoS propagation on-chip.

1) Reflection: We consider first the reflection at the interface between two material layers. If we denote r_1 as the distance between the transmitter and the reflecting point or reflector, and r_2 as the distance between the reflector and the receiver, then the frequency-dependent transfer function of the reflected ray propagation, H_{ref}, is given by:

$$H_{ref}(f,d) = r'_{TE}\left(\frac{\frac{c}{n}}{\sqrt{4\pi} f(r_1+r_2)}\right) e^{-j2\pi f \tau_{ref} - \frac{1}{2}K(f)(r_1+r_2)}, \tag{6}$$

where $\tau_{ref} = \frac{n(r_1+r_2)}{c}$ is the time-of-arrival of the reflected ray and r'_{TE} is the modified reflection coefficient according to the Kirchhoff scattering theory [28]. Here, we focus on the Transverse Electric (TE) part of the EM wave since its perpendicular to the plane of incidence, but a similar analysis can be conducted for Transverse Magnetic (TM) modes. The modified reflection coefficient captures the reduction of the signal power in the specular direction and for rough surfaces it is given by [29]:

$$r'_{TE} = \rho r_{TE}, \tag{7}$$

where r_{TE} is the Fresnel reflection coefficient for a smooth surface and ρ is the Rayleigh roughness factor:

$$\rho = e^{-\frac{g}{2}}, \tag{8}$$

$$g = \left(\frac{4\pi f \sigma \cos\theta_i}{\frac{c}{n}}\right)^2, \tag{9}$$

where θ_i is the angle of incidence and σ is the standard deviation of the surface roughness. In our analysis, we consider that the interface between two material layer is effectively smooth, i.e., $\sigma \leq \frac{\lambda}{10}$. Finally, r_{TE} is given by:

$$r_{TE} = \frac{Z_0 \cos\theta_i - Z\cos\theta_t}{Z_0\cos\theta_i + Z\cos\theta_t}, \tag{10}$$

where θ_t is the angle of refraction:

$$\theta_t = \sin^{-1}\left(\frac{Z_0}{Z}\sin\theta_i\right), \tag{11}$$

$Z_0 = 377\ \Omega$ is the free space wave impedance and Z is the wave impedance of the SiO_x. This is can be obtained as [28]:

$$Z = \frac{Z_0}{\sqrt{n^2 - \left(\frac{K\lambda}{4\pi}\right)^2 - j\frac{2nK\lambda}{4\pi}}}, \tag{12}$$

where λ is wavelength of incident wave. r_{TE} is illustrated in Fig. 3(a). These rays are depicted in Fig. 4(b).

2) Diffraction: In our scenario, diffraction appears when the radiated EM wave is obliquely incident on the edge of one of the cores on chip. The diffraction channel transfer function, H_{dif}, is given by:

$$H_{dif}(f,d) = D\left(\frac{\frac{c}{n}}{\sqrt{4\pi} f(d_1+d_2)}\right) e^{-j2\pi f \tau_{dif} - \frac{1}{2}K(f)(d_1+d_2)}, \tag{13}$$

where the diffraction coefficient, D, characterizes the loss that is created in addition to the LoS propagation attenuation, d_1 is the distance between the transmitter and the diffracting point, d_2 is the distance between the diffracting point and the receiver, and $\tau_{dif} = \frac{n(d_1+d_2)}{c}$ is the time-of-arrival of the diffracted ray.

The diffraction coefficient D can be mathematically obtained by means of geometrical theory of diffraction, which is an extension of geometrical optics [30, 31]. We focus on the case in which the radiated EM wave is obliquely incident on an edge of an element with finite conductivity. Given that the medium being considered is homogenous, the diffracted ray is still a straight line (i.e., it does not bend).

First, we consider the two-dimensional case in which the edge is a point on a straight line and the incident rays lie in planes normal to the edge. Let us consider only one of

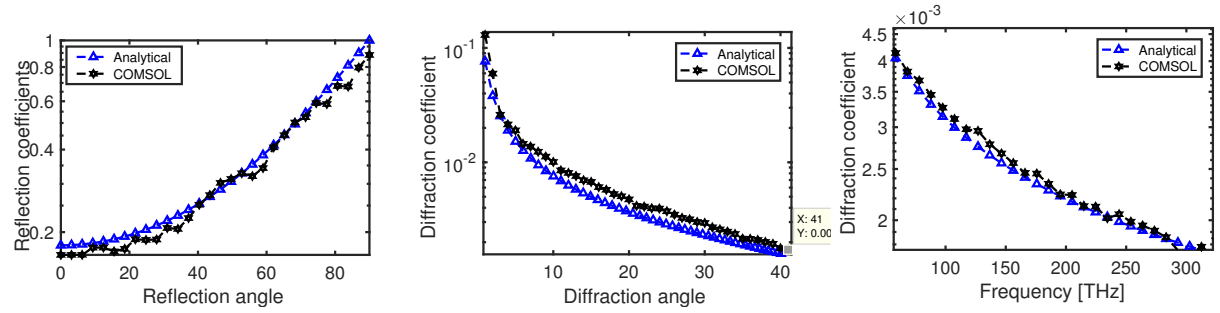

(a) (b) (c)

Fig. 3. a) Reflection coefficient r_{TE} (10) at 193 THz, b) Diffraction coefficient D (13) at 193 THz, c) Diffraction coefficient D (13) at $\phi' = 30$ °. Simulations with COMSOL Multi-physics, as described in Sec. III, are conducted to validate the analytical models.

such planes, which contains both the incident ray and the diffracted ray. These rays are depicted in Fig. 4(c) (side view) and Fig. 4(d) (top view). The incident ray can be described in spherical coordinates as (d_1, β_0, ϕ') and, similarly, the coordinates of the diffracted ray are given by $(d_2, \pi - \beta_0, \phi)$. β_0 refers to the grazing and near grazing incidence along the edge or the angle between the incident ray and the edge ($\frac{\pi}{2}$ in this case). The angles between the incident and diffracted rays and the tangent to the surface are ϕ and ϕ', respectively. Here the wedge angle is $(2-\eta)\pi$. If $\eta = \frac{1}{2}$, the wedge has interior right angle, if $\eta = \frac{1}{M}, M = 3, 4, 5, ...$, we have interior acute angles. If $\eta = 1$, the edge vanishes for the entire plane.

For this geometry and notation, the diffraction coefficient is given by [30, 31]:

$$\begin{aligned} D(\phi, \phi', \beta_0) = & \frac{-\exp[-j(\frac{\pi}{2})]}{2n\sqrt{2\pi k}\sin\beta_0} \\ & \cdot [\cot\left(\frac{\pi + (\phi - \phi')}{2n}\right) F[kLa^+(\phi - \phi')] \\ & + \cot\left(\frac{\pi + (\phi - \phi')}{2n}\right) F[kLa^-(\phi - \phi')] \\ & \pm (\cot\left(\frac{\pi + (\phi + \phi')}{2n}\right) F[kLa^+(\phi + \phi')] \\ & + \cot\left(\frac{\pi + (\phi + \phi')}{2n}\right) F[kLa^-(\phi + \phi')])], \end{aligned} \tag{14}$$

where k is the wave vector,

$$F(X) = 2j\sqrt{X}\exp(jX)\int_{\sqrt{X}}^{\infty}\exp(-j\tau^2)d\tau, \tag{15}$$

which involves the Fresnel equation, and

$$a^{\pm}(\beta) = 2\cos^2\left(\frac{2n\pi N^{\pm} - (\beta)}{2}\right) \tag{16}$$

is a measure of the angular separation between the field point and a shadow or diffraction boundary, in which $N^{\pm}$ are the integers which satisfy the following equations:

$$2n\pi N^+ - (\beta) = \pi, 2n\pi N^- - (\beta) = -\pi \tag{17}$$

with

$$\beta = \phi \pm \phi'. \tag{18}$$

It is apparent that N^+, N^- each have two values. L is a distance parameter, which can be determined for several types of illumination. Here for spherical-wave incidence we have:

$$L = \frac{d_1 d_2}{d_1 + d_2}\sin^2\beta_0. \tag{19}$$

The diffraction coefficient D is illustrated in Fig. 3(b) and (c) as a function of diffraction angle and frequency respectively.

C. Multi-path Model

By combining the above models in (1), (6), and (13), the multi-ray model can be rearranged as:

$$\begin{aligned} H(f,d) = & \left|\frac{\frac{c}{n}}{\sqrt{4\pi}fd_{LoS}}\exp\left(-\frac{1}{2}K(f)d_{LoS}\right)\right| \\ & + \sum_{q=1}^{N_{ref}}\left|r'_{TE}\left(\frac{\frac{c}{n}}{\sqrt{4\pi}f(r_1+r_2)}\right)e^{\frac{-1}{2}K(f)(r_1+r_2)}\right|_q \\ & + \sum_{u=1}^{N_{dif}}\left|D\left(\frac{\frac{c}{n}}{\sqrt{4\pi}f(d_1+d_2)}\right)e^{\frac{-1}{2}K(f)(d_1+d_2)}\right|_u, \end{aligned} \tag{20}$$

where N_{ref} is the total number of reflected rays and N_{dif} is the total number of diffracted rays. The presence of LoS as well as the number of reflected and diffracted rays depend on the specific chip geometry, such as thickness and arrangement of layers and number and location of cores, among others.

III. Simulation and Numerical Results

In this section, we validate the developed analytical model for on-chip wireless optical communication by means of EM simulations. Then, by utilizing the developed model, we analyze the total channel response and path-loss as a function of frequency and distance.

A. Model Validation

We utilize COMSOL Multi-physics to simulate the propagation of wireless optical signals in a multi-layered heterostructure such as that given in Fig. 1, with the specified thickness and material properties for each layer. An ideal on-chip optical source is emulated by means of an active arctic port. The signal at different distances is measured by means of

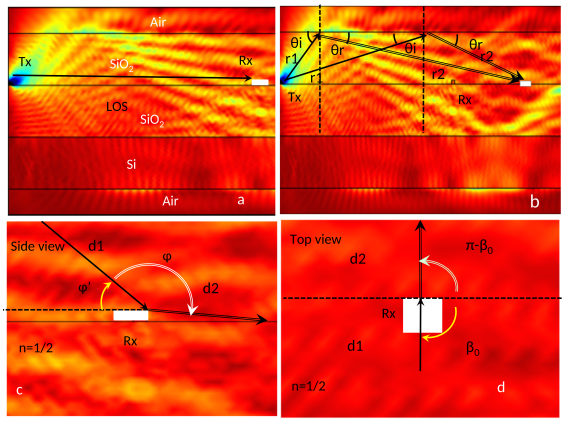

Fig. 4. Propagation models between the transmitter (Tx) and the receiver (Rx). (a) Line-of-sight or direct ray propagation. (b) Reflected ray propagation. (c) Diffracted ray propagation from side view at wedge with $n = \frac{1}{2}$. (d) Diffracted ray propagation from top view at wedge with $n = \frac{1}{2}$.

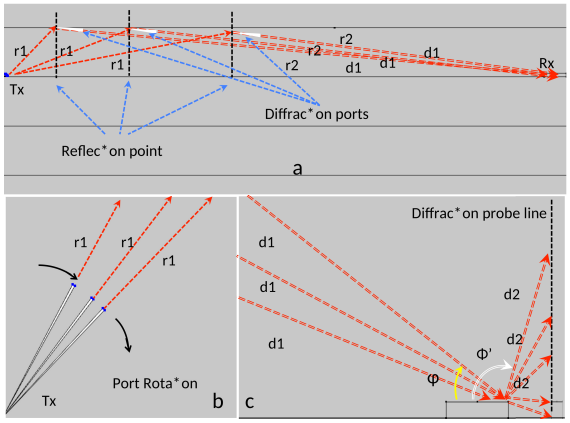

Fig. 5. Ray tracing simulation from transmitter to receiver. (a) Reflected and diffracted ray tracing. (b) Port rotation at transmitter. (c) Diffraction edge and ray tracing at the edge.

point probes. A frequency-domain EM simulation is conducted between 50 THz and 300 THz (λ between 1 and 6 μm).

First, we focus on the analysis of the system response at a fixed distance of $d = 40$ μm. In Fig. 6, we illustrate the channel frequency response $|H(f,d)|^2$ both simulated with COMSOL and analytically obtained from (20). For the analytical model, we extract the reflection and diffraction points from the simulation, and utilize (6) and (13) to compute the paths strength at the receiver.

More specifically, in our simulations, we define a quarter circular arc port to emulate the radiation of an omnidirectional nano-antenna. This is then divided into narrower sub-arcs to perform ray tracing calculations of the reflected and diffracted rays. We set the number of these sub-arcs (N_{ref} and N_{dif}) to an arbitrarily large number (100 in these results) for accuracy. Note that this number could be reduced to reduce the computational complexity, at the cost of lower accuracy. For each sub-arc value, the radiated ray r_1 and its reflected ray r_2 are obtained by finding the reflection point at the boundary. Knowing the thickness of the layer, the port angle and the position of both the transmitter and the receiver, r_1 and its reflected ray r_2 are obtained using trigonometry. This task is done for each ray, i.e., N_{ref} times until we calculate all reflected rays. A similar strategy is followed for the computation of the diffracted rays, but now starting from the both LoS and the reflected rays. In particular, the rays r_2 are now d_1 in our diffraction calculations. From the position of the sub-arc and their angle, the incident angles ϕ' at the edge of the core are obtained. We define a line across the layer as a lets say probe to see which point has the highest value of signal to keep it as the of diffracted ray path and its position. By knowing that angle of diffraction ϕ and d_2 are obtained. This task is done N_{dif} times. Fig. 5 illustrates the described procedure.

After the validation of the propagation properties, we numerically investigate the path loss.

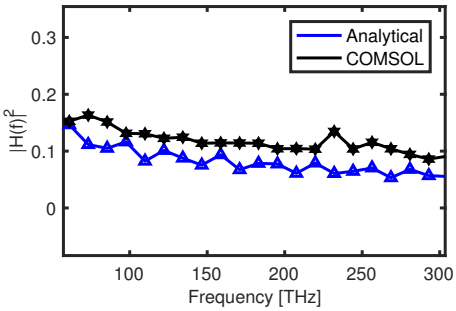

Fig. 6. Channel frequency response $|H(f)|^2$ at $d = 40\mu m$.

B. Path Loss

We utilize the developed channel model to analyze the path loss at optical frequencies on chip. In Fig. 7, the total path loss is shown as a function of frequency and for different transmission distances, which is given in dB by

$$A(f,d) = 20\log\left(\frac{1}{H(f,d)}\right) \tag{21}$$

where H is the channel frequency response given by (20). The path loss can easily go above 100 dB for transmission distances in the order of just a 100 μm. Total path loss increases with both the distance and the frequency and decreases with increasing oxygen content of SiO_x due to its absorption coefficient. The fluctuation in the path-loss is mainly related to the constructive or destructive addition of the reflected and diffracted rays at the receiver points. By increasing the distance, the fluctuation decrease such that if we only calculate the LOS signal, we will have smooth figure for path-loss.

IV. Conclusions and Future Work

On-chip wireless optical communication among cores has been proposed as a mechanism to enable high-speed, multicast and broadcast links for control signaling and data sharing in WNoC. In this paper, the first steps towards assessing the feasibility of this new communication and networking paradigm

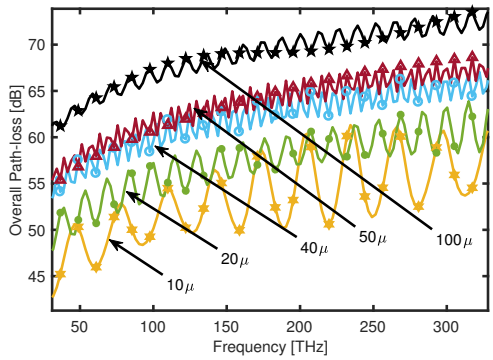

Fig. 7. Path loss of the wireless optical channel as a function of frequency for different transmission distances.

have been taken. In particular, we have developed the first multi-path channel model for wireless optical communication on-chip, by taking into account the spreading and absorption in silicon for line-of-sight propagation and, in addition, the reflection at the layer interfaces and diffraction at the cores' edges for non-line-of-sight propagation. The developed model has been validated in a specific on-chip scenario by means of electromagnetic simulations, and path-loss numerical calculations have been developed to analyze the feasibility of this technology. The results show that optical wireless links on chip for up to several millimeter distances are possible, in part thanks to the reflected rays. Our future work includes a time-domain analysis of the channel and the study of delay spread and coherence bandwidth, prior to the development of tailored physical layer solutions.

Acknowledgments

This work was supported by the U.S. National Science Foundation (NSF) under Grants No. CBET-1445934 and No. CBET-1555720.

References

[1] W. J. Dally and B. Towles, "Route packets, not wires: on-chip interconnection networks," in *Design Automation Conference, 2001. Proceedings*. IEEE, 2001, pp. 684–689.

[2] L. Benini and G. De Micheli, "Networks on chips: a new soc paradigm," *computer*, vol. 35, no. 1, pp. 70–78, 2002.

[3] A. W. Topol, D. La Tulipe, L. Shi, D. J. Frank, K. Bernstein, S. E. Steen, A. Kumar, G. U. Singco, A. M. Young, K. W. Guarini *et al.*, "Three-dimensional integrated circuits," *IBM Journal of Research and Development*, vol. 50, no. 4.5, pp. 491–506, 2006.

[4] E. Socher and M.-C. F. Chang, "Can rf help cmos processors?[topics in circuits for communications]," *IEEE Communications Magazine*, vol. 45, no. 8, pp. 104–111, 2007.

[5] R. G. Beausoleil, P. J. Kuekes, G. S. Snider, S.-Y. Wang, and R. S. Williams, "Nanoelectronic and nanophotonic interconnect," *Proceedings of the IEEE*, vol. 96, no. 2, pp. 230–247, 2008.

[6] D. W. Matolak, A. Kodi, S. Kaya, D. DiTomaso, S. Laha, and W. Rayess, "Wireless networks-on-chips: architecture, wireless channel, and devices," *IEEE Wireless Communications*, vol. 19, no. 5, pp. 58–65, 2012.

[7] D. Zhao and Y. Wang, "Mtnet: design of a wireless test framework for heterogeneous nanometer systems-on-chip," *IEEE transactions on very large scale integration (VLSI) systems*, vol. 16, no. 8, pp. 1046–1057, 2008.

[8] S. Abadal, B. Sheinman, O. Katz, O. Markish, D. Elad, Y. Fournier, D. Roca, M. Hanzich, G. Houzeaux, M. Nemirovsky *et al.*, "Broadcast-enabled massive multicore architectures: a wireless rf approach," *IEEE micro*, vol. 35, no. 5, pp. 52–61, 2015.

[9] S. Abadal, E. Alarcón, A. Cabellos-Aparicio, M. C. Lemme, and M. Nemirovsky, "Graphene-enabled wireless communication for massive multicore architectures," *IEEE Communications Magazine*, vol. 51, no. 11, pp. 137–143, 2013.

[10] P. Bharadwaj, B. Deutsch, and L. Novotny, "Optical antennas," *Advances in Optics and Photonics*, vol. 1, no. 3, pp. 438–483, 2009.

[11] J. Dorfmuller, R. Vogelgesang, W. Khunsin, C. Rockstuhl, C. Etrich, and K. Kern, "Plasmonic nanowire antennas: experiment, simulation, and theory," *Nano letters*, vol. 10, no. 9, pp. 3596–3603, 2010.

[12] A. Alù and N. Engheta, "Wireless at the nanoscale: optical interconnects using matched nanoantennas," *Physical review letters*, vol. 104, no. 21, p. 213902, 2010.

[13] L. Feng, Z. J. Wong, R.-M. Ma, Y. Wang, and X. Zhang, "Single-mode laser by parity-time symmetry breaking," *Science*, vol. 346, no. 6212, pp. 972–975, 2014.

[14] L. Feng, Y.-L. Xu, W. S. Fegadolli, M.-H. Lu, J. E. Oliveira, V. R. Almeida, Y.-F. Chen, and A. Scherer, "Experimental demonstration of a unidirectional reflectionless parity-time metamaterial at optical frequencies," *Nature materials*, vol. 12, no. 2, pp. 108–113, 2013.

[15] L. Feng, M. Ayache, J. Huang, Y.-L. Xu, M.-H. Lu, Y.-F. Chen, Y. Fainman, and A. Scherer, "Nonreciprocal light propagation in a silicon photonic circuit," *Science*, vol. 333, no. 6043, pp. 729–733, 2011.

[16] A. Nafari, C. C. Bowland, and H. A. Sodano, "Ultra-long vertically aligned lead titanate nanowire arrays for energy harvesting in extreme environments," *Nano Energy*, vol. 31, pp. 168–173, 2017.

[17] ——, "Vertically aligned lead titanate nanowire arrays for high temperature energy harvesting," in *ASME 2015 Conference on Smart Materials, Adaptive Structures and Intelligent Systems*. American Society of Mechanical Engineers, 2015, pp. V002T07A018–V002T07A018.

[18] Z. Vafapour, "Near infrared biosensor based on classical electromagnetically induced reflectance (cl-eir) in a planar complementary metamaterial," *Optics Communications*, vol. 387, pp. 1–11, 2017.

[19] M. Jafari and M. Rais-Zadeh, "Zero-static-power phase-change optical modulator," *Optics letters*, vol. 41, no. 6, pp. 1177–1180, 2016.

[20] C. Han, A. O. Bicen, and I. F. Akyildiz, "Multi-ray channel modeling and wideband characterization for wireless communications in the terahertz band," *IEEE Transactions on Wireless Communications*, vol. 14, no. 5, pp. 2402–2412, 2015.

[21] H. Guo, P. Johari, J. M. Jornet, and Z. Sun, "Intra-body optical channel modeling for in vivo wireless nanosensor networks," *IEEE transactions on nanobioscience*, vol. 15, no. 1, pp. 41–52, 2016.

[22] COMSOL Multiphysics Simulation Software. COMSOL. [Online]. Available: http://www.comsol.com/products/multiphysics/

[23] G. Cody, T. Tiedje, B. Abeles, B. Brooks, and Y. Goldstein, "Disorder and the optical-absorption edge of hydrogenated amorphous silicon," *Physical Review Letters*, vol. 47, no. 20, p. 1480, 1981.

[24] J. Tauc, R. Grigorovici, and A. Vancu, "Optical properties and electronic structure of amorphous germanium," *physica status solidi (b)*, vol. 15, no. 2, pp. 627–637, 1966.

[25] M. Nafari and J. M. Jornet, "Metallic plasmonic nano-antenna for wireless optical communication in intra-body nanonetworks," in *Proceedings of the 10th EAI International Conference on Body Area Networks*. ICST (Institute for Computer Sciences, Social-Informatics and Telecommunications Engineering), 2015, pp. 287–293.

[26] Z. Vafapour and M. Forouzeshfard, "Disappearance of plasmonically induced reflectance by breaking symmetry in metamaterials," *Plasmonics*, pp. 1–12, 2016.

[27] N. Ravindra and J. Narayan, "Optical properties of amorphous silicon and silicon dioxide," *Journal of applied physics*, vol. 60, no. 3, pp. 1139–1146, 1986.

[28] R. Vaughan and J. B. Andersen, *Channels, propagation and antennas for mobile communications*. Iet, 2003, vol. 50.

[29] R. Piesiewicz, C. Jansen, D. Mittleman, T. Kleine-Ostmann, M. Koch, and T. Kurner, "Scattering analysis for the modeling of thz communication systems," *IEEE Transactions on Antennas and Propagation*, vol. 55, no. 11, pp. 3002–3009, 2007.

[30] J. B. Keller, "Geometrical theory of diffraction," *JOSA*, vol. 52, no. 2, pp. 116–130, 1962.

[31] R. G. Kouyoumjian and P. H. Pathak, "A uniform geometrical theory of diffraction for an edge in a perfectly conducting surface," *Proceedings of the IEEE*, vol. 62, no. 11, pp. 1448–1461, 1974.